

# Role of Water in the Lyotropic Liquid Crystalline Lithium Iodide–Iodine–Water–C<sub>12</sub>E<sub>10</sub> Mesophase as a Gel Electrolyte in a Dye-Sensitized Solar Cell

Ezgi Yılmaz Topuzlu, Burak Ulgut,\* and Ömer Dag\*



Cite This: *Langmuir* 2021, 37, 8305–8313



Read Online

ACCESS |



Metrics & More

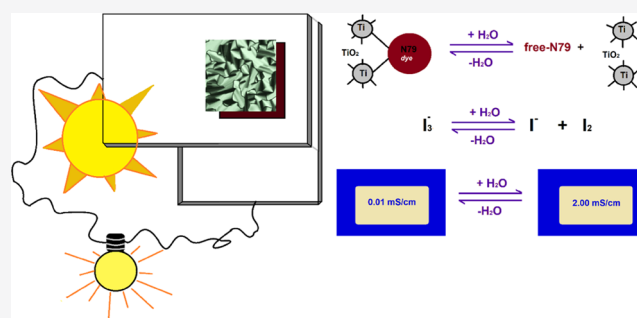


Article Recommendations



Supporting Information

**ABSTRACT:** By replacing volatile and flammable organic-based electrolytes with gel electrolytes, dye-sensitized solar cells (DSSCs) may be a viable and more practical alternative to other clean energy sources. Although they present a promising alternative, gel electrolytes still have some drawbacks for practical applications, such as low ionic conductivity and infusion difficulties into the pores of the working electrode. Here, we introduce a new one-step fabrication method that uses a lyotropic liquid crystalline (LLC) gel electrolyte (LiI:I<sub>2</sub>:H<sub>2</sub>O:C<sub>12</sub>H<sub>25</sub>(OCH<sub>2</sub>CH<sub>2</sub>)<sub>10</sub>OH) and a dye (N719) to construct a DSSC that performs (7.32%) 2.2 times better compared with a traditional two-step production. Water plays a key role in the gel electrolyte, where the H<sub>2</sub>O/LiI mole ratio is around 2.57 under ambient laboratory conditions (ALCs); however, this ratio linearly increases to 4.00 and then to 5.85 at 40 and 75% humidities, respectively, without affecting the two-dimensional (2D) hexagonal structure of the mesophase. The ionic conductivity of the gel electrolyte linearly increases accordingly, by 2.2 ( $4.8 \times 10^{-5}$  to  $10.6 \times 10^{-5}$ ) and 13.1 times ( $63.0 \times 10^{-5}$  S/cm) from ALC to 40 and ALC to 75% humidity, respectively. Increasing water in the gel phase improves the conductivity of the LLC mesophase and the short-circuit current ( $I_{sc}$ ) of the DSSC, but negatively influences the open-circuit voltage ( $V_{oc}$ ) of the cell, equilibrium reaction between the LiI and I<sub>2</sub>, and the anchoring of the dye molecules over the titania surface.



## INTRODUCTION

Efficiently harvesting renewable clean energy sources to overcome energy-related issues such as climate change and limited fossil fuel resources has been one of the most important challenges in the past decade. In this regard, the fabrication and improvement of the photovoltaic efficiencies of solar cells have attracted significant academic and industrial attention.<sup>1–9</sup> One promising and widely investigated solar cell is the dye-sensitized solar cell (DSSC).<sup>1,3,10–16</sup> A typical DSSC is constructed using a dye-sensitized (ruthenium-based dyes, N3 or N719, most common ones) titania-coated fluorine-doped tin oxide (FTO) glass anode, Pt nanoparticle-coated FTO glass counter electrode, and a LiI/I<sub>2</sub> acetonitrile solution as a redox couple (I<sup>−</sup>/I<sub>3</sub><sup>−</sup>) and electrolyte.



Acetonitrile is considered as the best solvent<sup>17</sup> because (i) acetonitrile has a low viscosity, (ii) solubility of LiI and I<sub>2</sub> is high, (iii) equilibrium constant,  $K_{eq}$  (where  $K_{eq} = [I_3^{-}]/([I^{-}] * [I_2])$ ) of eq 1 is high (favoring I<sub>3</sub><sup>−</sup> formation), and (iv) I<sub>3</sub><sup>−</sup> ion has a high diffusion coefficient in acetonitrile. Moreover, the open-circuit voltage ( $V_{oc}$ ), short-circuit current ( $I_{sc}$ ), and fill factor (FF) are all considerably high in acetonitrile-based electrolytes due to the absence of mass

transport limitations in the photochemical processes.<sup>17–20</sup> The I<sub>3</sub><sup>−</sup> generation is very fast and displays a more negative reduction potential in solvents that act as Lewis bases (such as acetonitrile).<sup>19</sup> However, acetonitrile is volatile and flammable, which are undesirable properties for practical applications. Water or ethanol have been also investigated widely as solvents and the electrolyte media.<sup>21–25</sup> There are many limitations associated with water as a medium for the I<sup>−</sup>/I<sub>3</sub><sup>−</sup> electrolyte in DSSCs. An enhanced exchange reaction occurs between water and anchored dye molecules on the working electrode, where the dye concentration is reduced significantly and the  $V_{oc}$  value is lower in aqueous media due to enhanced reverse reaction of eq 1 (due to smaller  $K_{eq}$ , over 10 000 times less in water compared to acetonitrile).<sup>26</sup> To overcome their limitations and improve the cell efficiency, water-mediated electrolytes have been widely investigated.<sup>21–25</sup> Regardless of the solvent, liquid electrolytes present other issues such as leakage and volatility.

Received: April 21, 2021

Revised: June 15, 2021

Published: June 29, 2021



Gel electrolytes, and electrolytes of deep eutectic solvents, which are not as volatile and relatively more stable have also been investigated.<sup>10,27–37</sup> However, the best cells, constructed using acetonitrile-based electrolytes display solar cell efficiencies of 14.2% that is 9.61% in a cell constructed using a gel-based electrolyte.<sup>35,38</sup> These need further improvement to be the potential electrolyte of DSSCs.<sup>35,39</sup>

In our previous studies, it has been shown that a LiX salt ( $X$  could be  $\text{Cl}^-$ ,  $\text{Br}^-$ ,  $\text{I}^-$ ,  $\text{NO}_3^-$ , and  $\text{CF}_3\text{SO}_3^-$ ), a nonionic surfactant, and a small amount of water form a lyotropic liquid crystalline (LLC) mesophase and may be used as an electrolyte in various electrochemical cells.<sup>40–44</sup> The  $\text{LiI}-\text{I}_2$  redox couple, used in DSSCs, and 10-lauryl ether ( $\text{C}_{12}\text{H}_{25}(\text{OCH}_2\text{CH}_2)_{10}\text{OH}$ , denoted as  $\text{C}_{12}\text{E}_{10}$ ) also form an LLC mesophase and could be used as a gel electrolyte in DSSCs.<sup>41</sup> The major issue of the LLC gel electrolytes is that it is difficult to effectively combine the gel electrolyte and DSSC electrodes. This lyotropic liquid crystalline gel electrolyte (LLC-GE) has an infusion problem (due to high viscosity); therefore, introducing it as a gel results in a limited electrode and electrolyte contact. However, introducing the electrolyte as a solution, by first dissolving the LLC-GE components in an excess water/ethanol mixture, improves the infusion and gelation into the pores of the anode electrode, the solar cell efficiency (by 33 times, from 0.1 to 3.33%), and cell parameters (fill factor (FF) of 0.69, open-circuit voltage ( $V_{\text{oc}}$ ) of 0.8 V, and short-circuit current ( $I_{\text{sc}}$ ) of 10 mA under 1.0 sun).<sup>41</sup>

Here, we are proposing a new method of introducing the  $\text{LiI}-\text{I}_2-\text{C}_{12}\text{E}_{10}$  gel electrolyte to the DSSCs by combining the dye and electrolyte addition steps and adjusting the amount of water in the gel electrolytes by controlling the humidity. The new approach improved the cell efficiency by another 2.2 times (from 3.33 to 7.32%). Increasing the amount of water in the gel electrolyte increased the short-circuit current density ( $J_{\text{sc}}$ ) to 7.53 mA/cm<sup>2</sup> under 0.3 sun. By introducing electrolyte and dye in a single step (new working electrode fabrication method), the highest  $V_{\text{oc}}$  value of 0.81 V was recorded, which is unusual in water-based electrolytes. Considering this performance increase, the role of water in the LLC-GEs was investigated using a balance, ALC conductivity, ART-FTIR spectroscopy, and UV–vis absorption spectroscopy techniques at various humidity levels.

## ■ EXPERIMENTAL SECTION

**Materials.** All chemicals and FTO (with a surface resistivity of  $\sim 7 \Omega/\text{sq}$ ) are of Sigma-Aldrich grade and used without further purification.

**Preparation of  $\text{LiI}-\text{I}_2$  Electrolyte Solution.** 10-Lauryl ether (1 g), LiI (0.43 g), and  $\text{I}_2$  (0.08 g) are dissolved in 5 mL of ethanol by stirring in a sealed vial on a magnetic stirrer for at least 6 h to produce a clear and homogeneous electrolyte solution.

**Preparation Protecting Layer Solution.** Titanium tetrabutoxide ( $\text{Ti}(\text{BuO})_4$ , 0.25 g) is dissolved in 5 mL of ethanol and acidified by adding 0.5 mL of concentrated nitric acid. The mixture is then stirred for at least 1 h on a magnetic stirrer to produce a homogeneous clear solution.

**Preparation of the  $\text{TiO}_2$  Paste.**  $\text{TiO}_2$  nanoparticles (0.2 g, average particle size of 21 nm), 12 drops of acetic acid, 1 drop of TritonX100, 0.6 mL of ethanol, and 0.6 mL of distilled water are put into a mortar and ground until the mixture becomes a paste.

**Preparation of the Dye Solution.** N719 (di-*tetra*-butylammonium *cis*-bis(isothiocyanato)bis(2,2'-bipyridyl-4,4'-dicarboxylato) ruthenium(II)) dye (0.024 g) is dissolved in 20 mL of ethanol to obtain a 1 mM dye solution, which is stirred or sonicated to produce a clear and homogeneous solution.

**Preparation of the Pt Solution.**  $\text{H}_2\text{PtCl}_6$  (0.026 g) is dissolved in 10 mL of ethanol and stirred until it becomes a clear and homogeneous solution.

**Preparation of Electrolyte Solution Using 4TBP.** A  $\text{LiI}-\text{I}_2$  electrolyte solution is prepared as described above, and then 15  $\mu\text{L}$  of 4-*tert*-butylpyridine (4TBP) is added to this solution and stirred for 10 min.

**Fabrication of the Working Electrode.** Fluorine-doped tin oxide (FTO, 2 by 1 cm dimensions) glasses are cleaned by washing using tap water, detergent, and then ethanol. After they are dried using pressurized  $\text{N}_2$  or dry air, a scotch tape is used to protect certain parts of the FTOs for a contact. The protecting layer solution is spread over the FTOs and spin-coated at 1000 rpm; then, the scotch tape is removed and calcined at 450 °C in a calcination oven for 15 min. The coated FTOs are again taped to have a 0.2 cm<sup>2</sup> area and then coated with freshly prepared titania paste using the doctor blading method and is again calcined at 450 °C for 1 h. Finally, the titania-coated FTOs are dipped into the 1 mM dye solution and kept overnight.

**Fabrication of the Counter Electrode.** FTO (2 cm  $\times$  2 cm) is cleaned by washing using tap water, detergent, and then ethanol. Once they are dried, the Pt solution is dropped (2–3 drops) and spread over the FTO and calcined at 450 °C for 1 h.

**Assembly of a DSSC.** The working electrode was removed from the dye solution and washed with ethanol to remove excess dye molecules. Then, the previously prepared  $\text{LiI}-\text{I}_2$  electrolyte solution was spread over the working electrode and kept under ambient conditions for the excess solvent to evaporate. The counter electrode was then put over the working electrode, and finally the cell was sealed by two clips.

**Characterization.** Polarized optical microscope (POM) images were obtained using a ZEISS Axio Scope A1 polarizing optical microscope. X-ray diffraction (XRD) patterns were collected using a Rigaku Miniflex diffractometer with a  $\text{Cu K}\alpha$  source operating at 30 kV/15 mA and wavelength of 1.54056 Å in the range of 1–5,  $2\theta$ , and 0.01 step size. Attenuated total reflectance–Fourier transform infrared (ATR-FTIR) spectra were recorded using Bruker ALPHA-P FTIR spectrometer with a diamond ATR attachment for the characterization of all samples at 4.0 cm<sup>-1</sup> resolution from 400 to 4000 cm<sup>-1</sup>. UV–vis spectra were recorded using a Varian Carry 5 double beam spectrophotometer. The spectra were collected with a speed of 600 nm/min and 0.2 nm resolution over a wavelength range of 200–800 nm. The AC impedance data were collected using a Gamry G750 potentiostat/galvanostat. A homemade cell was constructed using a 2 cm  $\times$  2 cm FTO glass scratched through with a diamond cutter to create a line. The scratched line was then filled with 0.01 M KCl to determine the cell constant. After cleaning the same cell, a drop of gel solution was placed over the line to determine the conductivity of the solution and gel (gelation is followed) using the predetermined cell constant. The AC impedance data were collected for five cycles using four different cells at room temperature (20–25 °C). The solar cell parameters were evaluated from the data collected using the DSSCs and an AM 1.5 solar simulator equipped with a 300 W xenon lamp (model no. 81172, Oriel). The light intensity was set to 300 W/m<sup>2</sup> using a reference Si photodiode. The  $I-V$  curves were obtained by applying an external bias to the cell and measuring the generated photocurrent using a Keithley model 2400 digital source meter. The water evaporation was monitored using a three-digit balance (Denver model IR-35). A known quantity of the electrolyte solution was dropped in a plastic sample holder over the balance, and the weight decrease was followed over time. A typical experiment takes a few hours to a day. The humidity conditions were set using either a humidity chamber (MMM Group Climacell CMC-111) that can be adjusted to any humidity or saturated salt solutions (with humidities of 11, 43, 52, 68, 75, and 84% for the saturated solutions of LiCl, NaBr, KI, NaCl, and KCl). The humidity-dependent ATR-FTIR and conductivity measurements were carried out using saturated salt solutions in a closed 50 and 500 mL containers over the ATR crystal and conductivity cell, respectively.

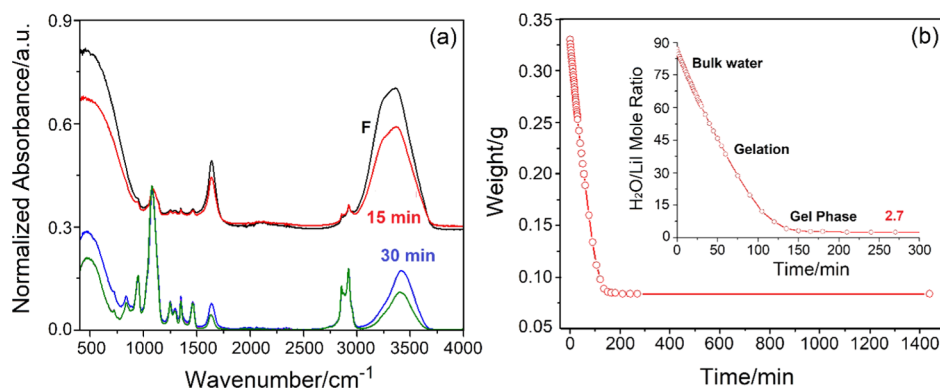


**Figure 1.** Evaporation of excess water from  $2\text{LiI} \cdot 0.2\text{I}_2 \cdot x\text{H}_2\text{O} \cdot \text{C}_{12}\text{E}_{10}$  solution, monitored using (a) ATR-FTIR (F stands for fresh solution) and (b) balance (inset is the  $\text{H}_2\text{O}/\text{LiI}$  mole ratio versus time plot).

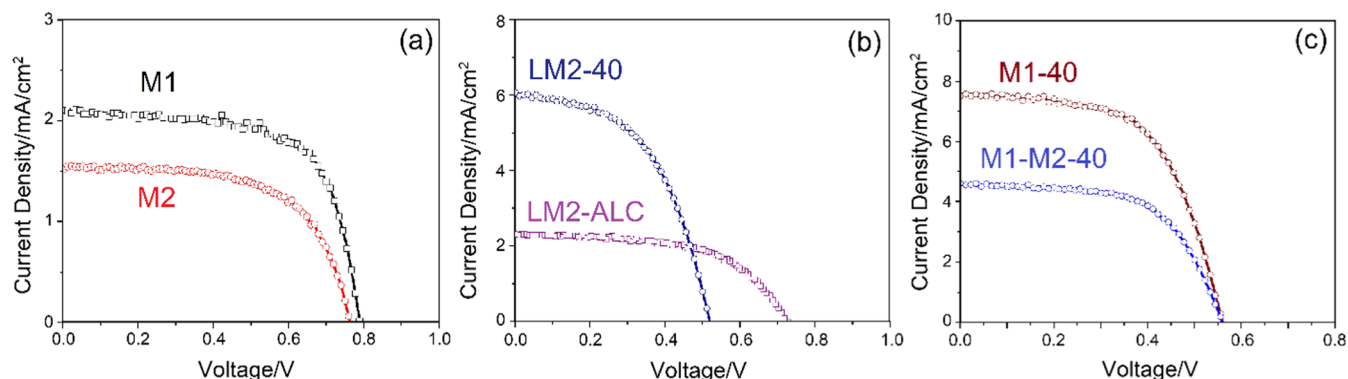


**Figure 2.**  $I$ - $V$  curves of the cells constructed using  $2\text{LiI} \cdot 0.2\text{I}_2 \cdot \text{C}_{12}\text{E}_{10}$  LLC-GE as electrolyte and methods: (a) M1 and M2, (b) LM2-ALC and LM2-40, and (c) combination of the new methods and humidity, M1-40 and M1-M2-40.

## RESULTS AND DISCUSSION

The evaporation of a homogeneous aqueous solution of LiI,  $\text{I}_2$ , and  $\text{C}_{12}\text{E}_{10}$  either by spin-coating over a substrate or by drop casting results in a lyotropic liquid crystalline gel electrolyte (LLC-GE). For example, a solution of 2:0.2:1:90, LiI: $\text{I}_2$ : $\text{C}_{12}\text{E}_{10}$ : $\text{H}_2\text{O}$ , produces LLC-GE with a 2:0.2:1:5.14 mole of LiI: $\text{I}_2$ : $\text{C}_{12}\text{E}_{10}$ : $\text{H}_2\text{O}$  after complete water evaporation. In such an experiment, the amount of water that remains in the LLC-GE depends on the ambient humidity (see below). The gel phase displays a focal conic fan texture under a polarized optical microscope (POM) and diffraction line(s) at small angle(s) in the X-ray diffraction (XRD) pattern; see Figure S1. Figure S1a shows two small-angle XRD patterns of  $2\text{LiI} \cdot 0.2\text{I}_2 \cdot x\text{H}_2\text{O} \cdot \text{C}_{12}\text{E}_{10}$  ( $x = 6$  and 8). The fan texture, observed over the POM image, is characteristic for a two-dimensional (2D) hexagonal mesophase that diffracts at  $2\theta = 2.0^\circ$ , originating from the (100) plane. The position of the diffraction line is sensitive to the amount of water in the mesophase and slightly shifts to lower angles with increasing water in the media. Aging an LLC sample or altering the LLC mesophase preparation method (directly as a gel or by evaporation of the excess solvent of a solution mixture) does not alter the structure or the usability of the mesophase as an LLC-GE in DSSCs.<sup>41</sup>

A 3.33% maximum efficiency from a DSSC, constructed using LLC LiI- $\text{I}_2$  redox electrolyte, was recorded previously.<sup>41</sup> Note that an LLC-GE can be directly prepared as a gel in the presence of about 3 mol  $\text{H}_2\text{O}$  per LiI; however, employing the LLC-GE as a gel causes an infusion problem due to its high viscosity. Introducing the electrolyte composition to DSSCs as a solution (ethanol or ethanol/water mixture) overcomes this

problem, resulting in an increase in the cell performance.<sup>39</sup> while excess solvent evaporates over the working electrode, where the gel electrolyte keeps its required amount of water (typically two to three water molecules per LiI; see below) and remains indefinitely stable. Also note that it has been previously shown that the LLC-GEs, prepared as gel or with excess solvent and solvent evaporation, are identical in terms of composition and structure.<sup>41</sup> However, fast solvent evaporation and gelation of the electrolyte before a complete infusion through the entire porous working electrode may result in an LLC-GE partially covering the working electrode surface; the gel infusion may still be a problem and needs further investigation. In this work, we overcome the infusion challenges to some extent by developing new approaches.

The LiI: $\text{I}_2$ : $\text{C}_{12}\text{E}_{10}$  electrolytes have been previously prepared with different salt/surfactant mole ratios and characterized by XRD and POM techniques.<sup>41,44</sup> The LLC-GEs with 4 and 5 LiI/ $\text{C}_{12}\text{E}_{10}$  mole ratios were also prepared and found to be semisolid soft mesocrystals<sup>41,44</sup> that may not be applicable as electrolyte in DSSCs. Increasing the amount of  $\text{I}_2$  in the mixture affects the properties of the LLC mesophase like viscosity, conductivity, etc.; the LiI/ $\text{I}_2$  mole ratio was kept at 10 to produce an effective electrolyte. The best solar cell parameters were obtained from a 2:0.2: $x$ :1, LiI: $\text{I}_2$ : $\text{H}_2\text{O}$ : $\text{C}_{12}\text{E}_{10}$ , LLC-GE.<sup>41</sup> Therefore, this electrolyte composition was further characterized by ATR-FTIR (see Figure 1a) and monitoring the solvent evaporation using a balance (see Figure 1b) and conductivity measurements. In approximately 30 min, the mesophase forms and becomes stable by losing excess water through evaporation. Figure 1a shows a set of ATR-FTIR

**Table 1. Summary of All Cell Parameters ( $I_{sc}$ ,  $V_{oc}$ , FF, and % efficiency ( $\eta$ ), Cells in Sets I, II, and III, Constructed Using Literature Method, LM2,<sup>41</sup> and the New Methods M1 and M2, Respectively) of the DSSCs**

cells	$J_{sc}$ (mA/cm <sup>2</sup> )	$V_{oc}$ (V)	FF	% $\eta$	cells	$J_{sc}$ (mA/cm <sup>2</sup> )	$V_{oc}$ (V)	FF	% $\eta$
set I <sup>a</sup>					set III <sup>c</sup>				
A	3.49	0.55	0.59	3.78	J	2.15	0.71	0.53	2.82
b	3.78	0.54	0.56	3.81	k	4.55	0.59	0.60	5.29
c	6.06	0.52	0.51	5.36	l	1.38	0.76	0.60	2.10
d	0.87	0.49	0.51	0.73	m	4.62	0.63	0.61	5.85
e	1.35	0.24	0.16	0.17	n	4.49	0.64	0.61	5.84
set II <sup>b</sup>									
f	1.53	0.77	0.63	1.86					
g	2.12	0.81	0.55	3.67					
h	4.61	0.56	0.60	5.14					
i	7.53	0.56	0.51	7.32					

<sup>a</sup>Set I cells, prepared using LM2 and sealed at (a) 70, (b) 60, (c) 40, (d) 30, and (e) 10% humidities. <sup>b</sup>Set II cells, prepared using new methods (M1-#, M2-#, and combination of M1-M2-#, where # is humidity at which these cells were sealed), (f) M2-ALC, (g) M1-ALC, (h) M1-M2-40, (i) M1-40. <sup>c</sup>Set III, cells were constructed with the adding 4TBP to the electrolyte solution in the new method and sealed at 40% humidity, (j) LM<sub>3</sub>-ALC, (k) LM<sub>3</sub>-40, (l) M1-ALC, (m) M1-40, and (n) M2-40.

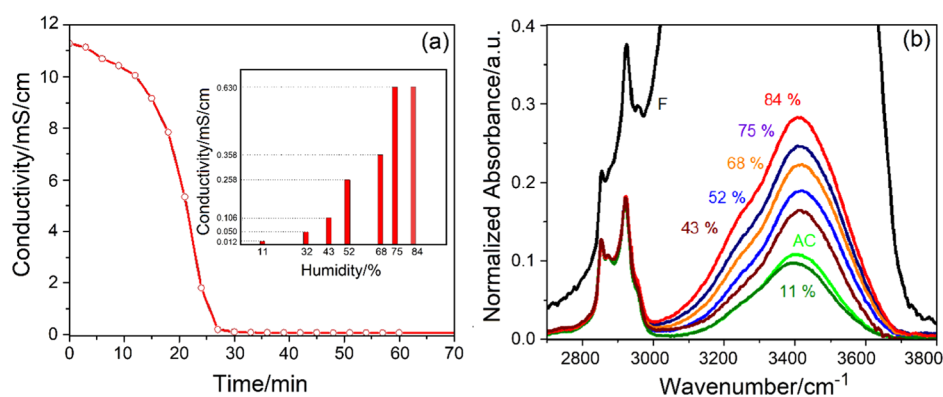


**Figure 3.** (a) Conductivity changes with evaporation of water from a 2LiI-0.2I<sub>2</sub>-xH<sub>2</sub>O-C<sub>12</sub>E<sub>10</sub> solution (inset shows the conductivity data at various humidity) and (b) normalized ATR-FTIR spectra at the indicated humidity level of 2LiI-0.2I<sub>2</sub>-xH<sub>2</sub>O-C<sub>12</sub>E<sub>10</sub> gels (F stands for fresh solution at time zero).

spectra; the upper two spectra (fresh and 15 min later) show the electrolyte in solution phase and the lower two spectra correspond to the LLC phase of LiI-I<sub>2</sub>-C<sub>12</sub>E<sub>10</sub>. The fresh sample displays intense peaks in the water stretching and bending regions at around 3354 and 1640 cm<sup>-1</sup>, respectively. These peaks lose intensity as the excess water evaporates, and the peak shape and position shift to 3410 and 1630 cm<sup>-1</sup>, respectively; see Figure 1a. The peak due to the water stretching mode blue-shifts, and the shoulder at 3240 cm<sup>-1</sup> loses its intensity during gelation (see Figure 1a) and originates from hydration water. Figure 1b shows the weight lost during the gelation process. It is clear in the weight versus time plot that the water evaporates in three or more steps: (i) evaporation of bulk water, (ii) evaporation during gelation, and (iii) further water evaporation from the gel phase. As shown in the inset of Figure 1b, the H<sub>2</sub>O/LiI mole ratio drops from 90 to 2.7 in 2 h and further drops to 2.57 in a stable gel phase under ambient laboratory condition (ALC).

We suggest two methods for effectively introducing the LLC-GE into a DSSC. The first method (M1) involves dipping a working electrode in a dye-electrolyte mixture and leaving it overnight in the mixture. In the second method (M2), the electrolyte solution is spread over a working electrode for a few minutes, followed by washing with ethanol and then dipping into a dye solution. The purpose of the new methods is to prevent any surface modification by the dye molecules that

may hinder the electrolyte infusion. Both M1 and M2 provided higher open-circuit voltage ( $V_{oc}$ ) values (see Figure 2a); the  $V_{oc}$  values increased from 600 to 809 and to 770 mV with FFs of 0.64 and 0.63, short-circuit currents of 0.24 and 0.304 mA, and cell efficiencies of 3.67 and 1.86%, respectively, under 0.3 sun power. A speculative reason for the improvements could be the fact that the dye molecules alter the surface properties of titania and cause a change in the infusion of electrolyte solution into the pores. Clearly, M1 works better than M2 and provides better solar efficiency. Therefore, M1 was used in further investigations.

To check the role of humidity, the electrolyte solution was first dropped over the working electrode using the method described in the literature<sup>41</sup> (denoted as LM1-#, where # is the % humidity) at 70% humidity in a humidity chamber at RT and then sealed after keeping the electrode until the electrolyte becomes a gel; then, the  $I$ - $V$  responses were recorded at ALC (varied between 16 and 20% humidity) RT (varies between 20 and 25 °C). This was repeated at each humidity level decreasing by 10% (from 70 to 10%) by keeping the cell sealed to ensure data collection from the same cell; see Figure S2. However, it is difficult to adjust the amount of water in the sealed cell to a level corresponding to the level of the humidity chamber. Clearly, humidity influences the cell performance (see Figure S2), but it is impossible to determine the amount of water in the cell at each humidity level using this approach.

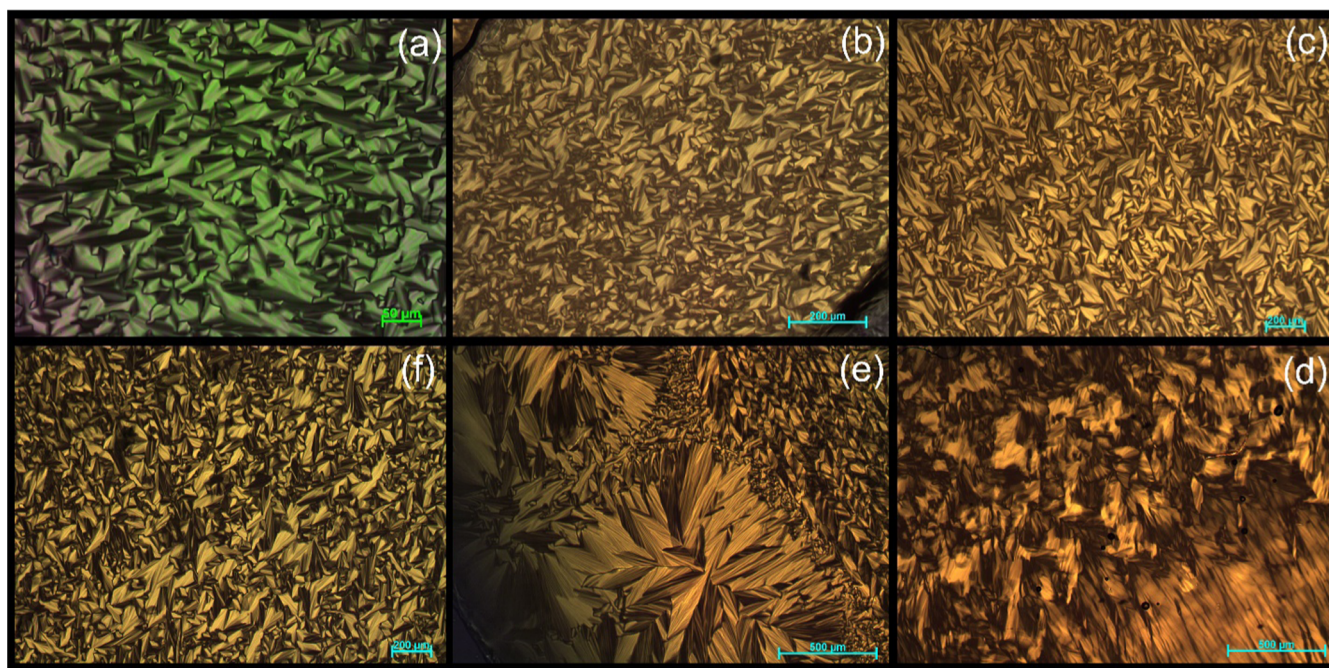


**Figure 4.** POM images of 2LiI-C<sub>12</sub>E<sub>10</sub> (a) and 2LiI-0.2I<sub>2</sub>-C<sub>12</sub>E<sub>10</sub> mesophase at percent humidities of (b) 30, (c) 40, (d) 50, (e) 60, and (f) 70.

However, the  $I$ - $V$  curves show that the cell releases water by decreasing humidity and performs accordingly. In a second set of experiments, different electrodes were used and sealed upon reaching equilibrium at each humidity level (10–70%, 6 different cells, labeled as LM2-#, where # is the % humidity level). Note that the amount of water in each cell is known in this set (see later). The cell parameters are tabulated in Table 1 (set 1). The cell, which is sealed at 10% humidity did not behave like a photodiode. However, the cell, sealed at 40% humidity level (LM2-40), displayed the best performance with an efficiency of 5.36%. This is 1.6 times higher than the previously recorded value from a similar cell.<sup>41</sup> The data set shows that the short-circuit currents and thus the efficiency of the cells is improved by adjusting the humidity.

Clearly, the most obvious reason could be an increase in the conductivity of the gel electrolyte. Figure 3a shows the conductivity versus time plot during evaporation of excess water of 2:0.2:90:1, LiI:I<sub>2</sub>:H<sub>2</sub>O:C<sub>12</sub>E<sub>10</sub>, solution. The high-conductivity region in the plot corresponds to the solution phase, and the low-conductivity region corresponds to the gel phase. The sharp decrease in between those two regions corresponds to the gelation process. The conductivity change becomes steady after 30 min and converges to  $7.8 \times 10^{-5}$  S/cm and further drops to  $4.8 \times 10^{-5}$  S/cm in 24 h (the water/LiI mole ratio drops to 2.57) and remains constant. The conductivity of the LLC-GE was also measured at various humidity levels using various saturated salt solutions, which provide a constant humidity around the conductivity setup. The saturated LiCl, NaBr, KI, NaCl, and KCl solutions provide 11, 43, 68, 75, and 84% humidity, respectively, in a closed small volume of space, where the sample is kept (see the Experimental Section for details on the measurements). The saturated salt solution was placed near the LLC-GE in the conductivity setup and was sealed from its surrounding and kept for 24 h to reach equilibrium with its surrounding prior to measurement. The conductivity of the gel electrolyte gradually increases with increasing humidity; see Figure 3b. It increases

from 0.1 mS/cm at 40% and to 0.6 mS/cm at around 75% humidity. Note that the cell performance is best at 40% humidity but declines at higher humidity values.

To determine the amount of water in the electrolyte at each humidity level, we also recorded ATR-FTIR spectra during water evaporation and under various humidity levels. Figure 3b shows the ATR-FTIR spectra recorded at specific humidity levels obtained using saturated LiCl (11%), NaBr (43%), K<sub>2</sub>CO<sub>3</sub> (52%), KI (68%), NaCl (75%), and KCl (84%) solutions. The spectra display a trend of increasing amount of water in LLC-GE with increasing humidity. The amount of water in the gel electrolyte, aged at ALC, contains 2.57 H<sub>2</sub>O/LiI and increases to around 4 H<sub>2</sub>O/LiI at 40% humidity; see Figure 3b. Note also that the humidity of ALC changes daily, as a result of which the amount of water in the gel phase changes, which can be observed in the ATR-FTIR spectrum. The H<sub>2</sub>O/LiI mole ratio increases linearly with increasing humidity and reaches 4.50 and 5.85 at 52 and 75% humidity levels, respectively. Also remember that further increasing water in the electrolyte creates other problem(s); it decreases the cell performance due to excess water, which behaves like bulk water (see below).

The 2LiI-0.2I<sub>2</sub>- $x$ H<sub>2</sub>O-C<sub>12</sub>E<sub>10</sub> LLC gel mesophase was further analyzed using POM under different humidities to check the structure of the mesophase. Figure 4 shows a set of POM images of 2LiI- $x$ H<sub>2</sub>O-C<sub>12</sub>E<sub>10</sub> and 2LiI-0.2I<sub>2</sub>- $x$ H<sub>2</sub>O-C<sub>12</sub>E<sub>10</sub> LLC mesophases, recorded at various humidity levels. Clearly, the addition of I<sub>2</sub> or the formation of I<sub>3</sub><sup>-</sup> ion in mesophase does not disturb the 2D hexagonal mesophase, as they display focal conic fan texture; see Figure 4a,b. The 2LiI-0.2I<sub>2</sub>- $x$ H<sub>2</sub>O-C<sub>12</sub>E<sub>10</sub> LLC samples were kept at 30, 40, 50, 60, and 70% humidity levels in the humidity chamber for several hours, and then their POM images were recorded after sealing them in the humidity chamber at those humidity levels; see Figure 4c–f, respectively. They all display focal conic fan textures that are characteristic for the 2D hexagonal mesophase. Therefore, the 2D hexagonal structure is not disturbed by the extra water (between 2.57 and

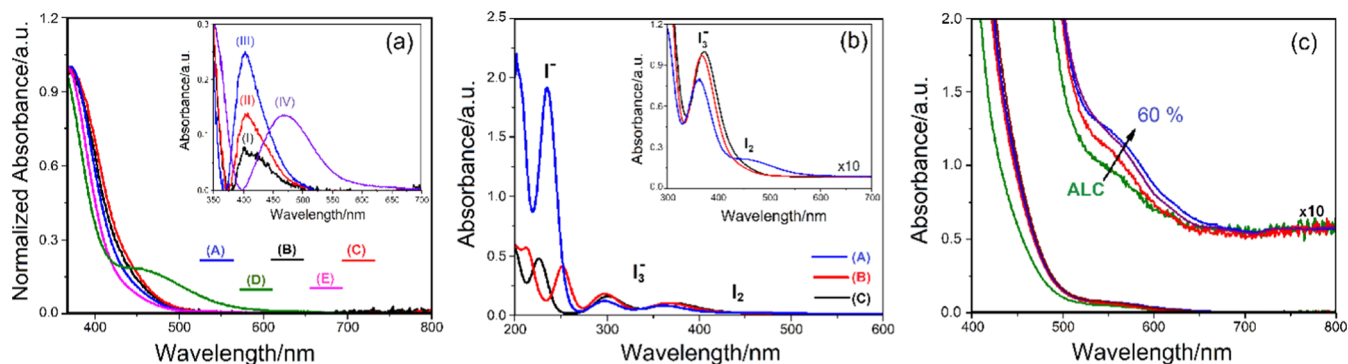


**Figure 5.** UV-vis absorption spectra of (a) 2:0.2:1: $x$ , LiI:I<sub>2</sub>:H<sub>2</sub>O:C<sub>12</sub>E<sub>10</sub> LLC-GE thin films at (A) ALC, (B) 50 and (C) 60% humidity, (D) 2LiI:I<sub>2</sub> in H<sub>2</sub>O, and (E) 2LiI:0.2I<sub>2</sub> in CH<sub>3</sub>CN; the inset displays the difference spectra of (I) (B) minus (A), (II) (C) minus (A), (III) (C) minus (E), and (IV) (D) minus (E); (b) an aqueous solution of 2LiI:0.2I<sub>2</sub> (A), an acetonitrile solution of 2LiI:0.2I<sub>2</sub> (B), and LLC-GE (C); the inset displays I<sub>3</sub><sup>-</sup> and I<sub>2</sub> regions multiplied by 10 of the same spectra; and (c) the solutions obtained by washing working electrodes after aging under ALC, 40, 50, and 60% humidities.

5.85 H<sub>2</sub>O/LiI) in the media and accords well with the trend in water evaporation followed by the balance experiment; see Figure 1b. Note also that the addition of 4-*tert*-butylpyridine (4TBP) does not also alter the structure (see later). In short, all samples with all additives display focal conic fan texture even after aging 12 months.

The  $I_{sc}$  and  $V_{oc}$  values of the DSSCs, constructed using LLC-GE, can be increased by controlling the humidity (water level in the LLC-GE) and by changing the preparation method of the working electrode, respectively. These two parameters were therefore combined to improve the solar cell performance; see Table 1 (set II). Figure 2c shows the  $I$ - $V$  curves of the two improved cells. Combining M1 and 40% humidity (M1-40) produces the best performing cells with a cell efficiency of 7.32%; see Figure 2c. However, combining M1, M2, and 40% humidity (M1-M2-40) provided a lower cell efficiency (5.14%); see Figure 2c and Table 1 (set II). Table 1 also shows the cell parameters of all sets (set I, constructed using the literature method,<sup>41</sup> and set II and set III cells, constructed using the new methods) tested in this work to compare the effect of each modification. Notice that the cells sealed at 40% humidity display the best performance of the three sets. We also employed M1 to test the cells at all humidity levels; see Figure S3. However, we found the same trend, i.e., 40% humidity always emerges to be the best humidity level for efficient cells.

To further improve the cell performance, 4-*tert*-butylpyridine (4TBP) has been used as an additive to modify the Fermi energy of titania and to block the titania surface sites to avoid shortcuts and thus increases the open-circuit potentials and short-circuit currents.<sup>45</sup> Therefore, 4TBP was also used together with the new methods (M1 and M2) to check whether the  $V_{oc}$  may be increased further. The working and counter electrodes were prepared as usual, but the LLC-GE was prepared by adding additional 4TBP to the electrolyte solution. The  $I$ - $V$  curves were collected, and cell parameters were evaluated using cells prepared under ALC and at 40% humidity; see Figure S4 and Table 1 (set III). However, the efficiency of the cells significantly decreased compared with the ones without 4TBP, indicating that the new method is not effective for incorporating 4TBP over the anode surface.

We suspected two possible reasons for the decrease in the cell efficiency with increasing humidity over 40%; one reason could be a change in the  $K_{eq}$  of eq 1 in favor of I<sub>2</sub> formation in

the LLC-GE (as it is the case in aqueous media), and the second reason may be an exchange reaction between excess water and anchored dye molecules over titania surface. To understand the effect of humidity, two different experiment sets were designed. The first set was designed to check the equilibrium constant. Iodine formation was investigated using a thin LLC-GE film (coated by spin coating of the electrolyte solution over a quartz substrate at 1000 rpm), which was kept in a humidity chamber at different humidity levels and by recording its UV-vis absorption spectra; see Figures 5a,b, and S4. The absorption spectrum of I<sub>2</sub> displays a characteristic peak at 463 nm in aqueous media with an extinction coefficient of 746 M/cm.<sup>46</sup> The extinction coefficients (calculated using Beer's law,  $A = \epsilon bc$ , where  $A$  is the absorbance at peak maxima,  $\epsilon$  is the extinction coefficient,  $b$  is the sample thickness, and  $c$  is the concentration) of the I<sub>3</sub><sup>-</sup> peaks (at 298 and 361 nm) and I<sup>-</sup> peak (at 219 nm) are  $4.0 \times 10^4$ ,  $2.64 \times 10^4$ , and  $1.34 \times 10^4$  M/cm, respectively.<sup>26,46-50</sup> Also note that the  $K_{eq}$  of eq 1 varies from solvent to solvent and it is 800 and  $10^7$  M<sup>-1</sup> in water and acetonitrile, respectively.<sup>26</sup>

The spectra of the LiI and I<sub>2</sub> mixture in LLC, water, and acetonitrile were also recorded to compare with each other; see Figure 5a,b, and S5. Both I<sup>-</sup> and I<sub>3</sub><sup>-</sup> peaks are sensitive to solvent and were observed at 235 and 361, 226 and 371, and 252 and 368 nm in aqueous, LLC, and acetonitrile solutions, respectively. The spectrum of aqueous solution of 2:1 Li:I<sub>2</sub> is also shown in Figure 5b to show the I<sub>2</sub> region, but even at such a high I<sub>2</sub> concentration, the I<sub>2</sub> peak is weakly visible in the spectrum of aqueous solution as a very weak shoulder on the low-energy tail of the intense I<sub>3</sub><sup>-</sup> peak. The spectra recorded in acetonitrile and LLC-GE do not display any intensity at around 463 nm (see Figure 5b), indicating a high equilibrium constant in both media for eq 1. Notice also that the low-energy tail of the I<sub>3</sub><sup>-</sup> peak is sensitive to the LiI/I<sub>2</sub> ratio in the LLC media, in which the tail due to I<sub>2</sub> increases in intensity by increasing the I<sub>2</sub>/LiI mole ratio; see Figure S4. Nevertheless, the I<sub>2</sub> peak does not appear as an obvious shoulder in the spectra of the LLC-GE samples. Figure 5a also displays two extra spectra, recorded using the 2:0.2: $x$ :1 (LiI:I<sub>2</sub>:H<sub>2</sub>O:C<sub>12</sub>E<sub>10</sub>) sample, kept at 50 ( $x$  is 8.4) and 60% humidity ( $x$  is 10.2). The spectra display peaks at around 298 and 371 nm due to triiodide ion with some changes on the low-energy tail around the iodine absorption region (see the difference spectra of various samples in the inset of Figure 5a), but it is still difficult

to assign these changes to the formation of  $I_2$  at a higher humidity. The  $K_{eq}$  values in the LLC-GE at various humidities using spectroscopic data were calculated using the spectroscopic data. Notice that  $K_{eq}$  is sensitive and linearly decreases with increasing humidity; it is ca.  $3.3 \times 10^4$ ,  $1.6 \times 10^4$ ,  $9.1 \times 10^3$ , and  $7.1 \times 10^3 \text{ M}^{-1}$  at 30, 40, 50, and 60% humidities, respectively. The change in  $K_{eq}$  clearly shows that increasing water in the media increases the  $I_2$  concentration in the gel phase; it increases by almost 4 times by increasing the humidity from ALC (around 16–20%) to 60%. An easier way to monitor the effect of extra water is to follow the change in the ratio of  $I^-$  absorbance at 226 nm ( $A_I$ ) to  $I_3^-$  absorbance at 371 nm ( $A_{TI}$ ).  $A_I/A_{TI}$  is inversely proportional with the equilibrium constant of eq 1, and it is around 100 in aqueous solution but drops to 4 in acetonitrile and ca. 5 in the LLC phase. Notice that  $A_I/A_{TI}$  increases with increasing humidity, showing an increase in the  $I_2$  formation. Moreover, the  $A_I/A_{TI}$  ratio is still far from the value of an aqueous solution and closer to the acetonitrile one, indicating that even though gel phase contains a large amount of water at higher humidities, water species (water ion) do not behave like bulk water for the equilibrium reaction between  $LiI$  and  $I_2$  (eq 1) in the LLC phase.

We also check the second possibility and further investigated the effect of humidity by designing another experiment using four different electrodes. The electrodes were prepared as usual and first dipped into a dye solution to coat their surface by dye molecules and washed well with ethanol to remove any unanchored dye molecule from the surface, then an electrolyte ethanol solution was dropped over each of those electrodes, and finally each electrode was kept at different humidities (ALC, 40, 50, and 60%) until gelation was complete. Each electrode was then washed with ethanol into separate vials; the solutions obtained contain the electrolyte, detached dye molecules (if any), and ethanol. Figure 5c shows the UV–vis absorption spectra of these solutions. The shoulder at around 533 nm corresponds to the N719 dye.<sup>51</sup> The peak due to dye absorption increases in the solutions as the humidity of the media increases. Since the dye molecules are further detached through exchange reaction with excess water at a higher humidity, it could be the other reason for the declined efficiencies for humidity over 40%, even though the conductivity of the electrolyte increases with extra water.

## CONCLUSIONS

A mixture of  $2LiI$ ,  $0.2I_2$ ,  $1C_{12}E_{10}$ , and  $90H_2O$  forms a clear solution that can be coated over a surface to lose its excess water to become a stable gel in a lyotropic liquid crystalline mesophase. The LLC mesophase reversibly absorbs at a higher humidity and desorbs water at a lower humidity. As a result, its ionic conductivity could be adjusted between 0.6 and 0.05 mS/cm and could be used as an LLC-GE in DSSCs. However, introducing LLC-GE into the DSSCs is challenging. Introducing the electrolyte in the solution phase together with the dye may partially or fully overcome this issue. Simply by changing the fabrication method of the working electrode and adjusting the amount of water in the electrolyte by aging the gel electrolyte at an appropriate humidity (typically around 40% humidity, until equilibrium is established), the efficiency of  $LiI/I_2$  LLC-GE based DSSCs could be enhanced by a factor of 2. This is mostly because of the nature of the LLC-GEs, since they hold extra water without altering the 2D hexagonal mesostructure, increasing conductivity and improving infusion

of the gel electrolyte into  $TiO_2$  pores result in a 7.32% efficiency. Excess water in the gel electrolyte has positive (by enhancing the conductivity of the electrolyte) and negative effects (by altering the electrolyte composition, favoring  $I_2$  formation as a result of lowering  $V_{oc}$  value and reducing the dye population over the titania anode surface as a result lowering  $I_{sc}$  value) to the overall DSSC performance. Further studies are necessary to improve the conductivity of the gel electrolytes by keeping the water amount in the LLC phase as low as possible using better conducting other  $LiX$  salts together with the  $I^-/I_3^-$  redox couple, but it is also a challenge for the development of LLC-GEs.

## ASSOCIATED CONTENT

### Supporting Information

The Supporting Information is available free of charge at <https://pubs.acs.org/doi/10.1021/acs.langmuir.1c01094>.

Additional  $I-V$  curves, XRD, POM, and UV–vis absorption spectra (PDF)

## AUTHOR INFORMATION

### Corresponding Authors

**Burak Ulgut** – Department of Chemistry, Bilkent University, 06800 Ankara, Turkey; UNAM—National Nanotechnology Research Center and Institute of Materials Science and Nanotechnology, Bilkent University, 06800 Ankara, Turkey; [orcid.org/0000-0002-4402-0033](https://orcid.org/0000-0002-4402-0033); Email: [ulgut@fen.bilkent.edu.tr](mailto:ulgut@fen.bilkent.edu.tr)

**Ömer Dag** – Department of Chemistry, Bilkent University, 06800 Ankara, Turkey; UNAM—National Nanotechnology Research Center and Institute of Materials Science and Nanotechnology, Bilkent University, 06800 Ankara, Turkey; [orcid.org/0000-0002-1129-3246](https://orcid.org/0000-0002-1129-3246); Email: [dag@fen.bilkent.edu.tr](mailto:dag@fen.bilkent.edu.tr)

### Author

**Ezgi Yılmaz Topuzlu** – Department of Chemistry, Bilkent University, 06800 Ankara, Turkey

Complete contact information is available at: <https://pubs.acs.org/doi/10.1021/acs.langmuir.1c01094>

### Author Contributions

The manuscript was written through contributions of all authors. All authors have given approval to the final version of the manuscript.

### Funding

TÜBİTAK 118Z820

### Notes

The authors declare no competing financial interest.

## ACKNOWLEDGMENTS

The authors thank TÜBİTAK (under the project number 118Z820) for the financial support of this work. Ö.D. is a member of the Science Academy, Istanbul, Turkey.

## ABBREVIATIONS USED

LLC-GE, lyotropic liquid crystalline gel electrolyte; DSSC, dye-sensitized solar cell; FF, fill factor;  $V_{oc}$ , open-circuit voltage;  $I_{sc}$ , short-circuit current; ALC, ambient laboratory condition

## REFERENCES

- (1) Kamat, P. V. Meeting the clean energy demand: nanostructure architectures for solar energy conversion. *J. Phys. Chem. C* **2007**, *111*, 2834–2860.
- (2) O'Regan, B.; Grätzel, M. A low-cost, high-efficiency solar cell based on dye-sensitized colloidal TiO<sub>2</sub> films. *Nature* **1991**, *353*, 737–740.
- (3) Grätzel, M. Photoelectrochemical cells. *Nature* **2001**, *414*, 338–344.
- (4) Lee, J.-K.; Yang, M. Progress in light harvesting and charge injection of dye-sensitized solar cells. *Mater. Sci. Eng. B* **2011**, *176*, 1142–1160.
- (5) Hagfeldt, A.; Boschloo, G.; Sun, L.; Kloo, L.; Pettersson, H. Dye-sensitized solar cells. *Chem. Rev.* **2010**, *110*, 6595–6663.
- (6) Kuang, D.; Wang, P.; Ito, S.; Zakeeruddin, S. M.; Grätzel, M. Stable mesoscopic dye-sensitized solar cells based on tetracyanoborate ionic liquid electrolyte. *J. Am. Chem. Soc.* **2006**, *128*, 7732–7733.
- (7) Wang, Q.; Ito, S.; Grätzel, M.; Fabregat-Santiago, F.; Mora-Sero, I.; Bisquert, J.; Bessho, T.; Imai, H. Characteristics of high efficiency dye-sensitized solar cells. *J. Phys. Chem. B* **2006**, *110*, 25210–25221.
- (8) Upadhyaya, H. M.; Senthilarasu, S.; Hsu, M. H.; Kumar, D. K. Recent progress and the status of dye-sensitized solar cell (DSSC) technology with state-of-the-art conversion efficiencies. *Sol. Energy Mater. Sol. Cells* **2013**, *119*, 291–295.
- (9) Omar, A.; Ali, M. S.; Rahim, N. A. Electron transport properties analysis of titanium dioxide dye-sensitized solar cells (TiO<sub>2</sub>-DSSCs) based natural dyes using electrochemical impedance spectroscopy concept: A review. *Sol. Energy* **2020**, *207*, 1088–1121.
- (10) An, H.; Xue, B.; Li, D.; Li, H.; Meng, Q.; Guo, L.; Chen, L. Environmentally friendly LiI/ethanol based gel electrolyte for dye-sensitized solar cells. *Electrochim. Commun.* **2006**, *8*, 170–172.
- (11) Tennakone, K.; Kumara, G. R. R. A.; Kumarasinghe, A. R.; Wijayantha, K. G. U.; Sirimanne, P. M. A dye-sensitized nano-porous solid-state photovoltaic cell. *Semicond. Sci. Technol.* **1995**, *10*, 1689–1693.
- (12) Kamat, P. V. Solar cells by design. *J. Phys. Chem. Lett.* **2010**, *1*, 3147–3148.
- (13) Cao, F.; Oskam, G.; Searson, P. C. A Solid state, dye sensitized photoelectrochemical cell. *J. Phys. Chem. A* **1995**, *99*, 17071–17073.
- (14) Kubo, W.; Makimoto, Y.; Kitamura, T.; Wada, Y.; Yanagida, S. Quasi-solid-state dye-sensitized solar cell with ionic polymer electrolyte. *Chem. Lett.* **2002**, *31*, 948–949.
- (15) Chiba, Y.; Islam, A.; Watanabe, Y.; Komiyama, R.; Koide, N.; Han, L. Dye-sensitized solar cells with conversion efficiency of 11.1%. *Jpn. J. Appl. Phys.* **2006**, *45*, L638–L640.
- (16) Grätzel, M. Solar energy conversion by dye-sensitized photovoltaic cells. *Inorg. Chem.* **2005**, *44*, 6841–6851.
- (17) Wu, J.; Lan, Z.; Lin, J.; Huang, M.; Huang, Y.; Fan, L.; Luo, G. Electrolytes in dye-sensitized solar cells. *Chem. Rev.* **2015**, *115*, 2136–2173.
- (18) Hauch, A.; Georg, A. Diffusion in the electrolyte and charge-transfer reaction at the platinum electrode in dye-sensitized solar cells. *Electrochim. Acta.* **2001**, *46*, 3457–3466.
- (19) Kebede, Z.; Lindquist, S. E. Donor-acceptor interaction between non-aqueous solvents and I<sub>2</sub> to generate I<sub>3</sub><sup>-</sup>, and its implication in dye sensitized solar cells. *Sol. Energy Mater. Sol. Cells* **1999**, *57*, 259–275.
- (20) Hara, K.; Horiguchi, T.; Kinoshita, T.; Sayama, K.; Arakawa, H. Influence of electrolytes on the photovoltaic performance of organic dye-sensitized nanocrystalline TiO<sub>2</sub> solar cells. *Sol. Energy Mater. Sol. Cells* **2001**, *70*, 151–161.
- (21) Xiang, W.; Huang, F.; Cheng, Y.-B.; Bach, U.; Spiccia, L. Aqueous dye-sensitized solar cell electrolytes based on the cobalt(II)/(III) tris(bipyridine) redox couple. *Energy Environ. Sci.* **2013**, *6*, 121–127.
- (22) Yang, Y.; Zhou, C. H.; Xu, S.; et al. Optimization of a quasi-solid-state dye-sensitized solar cell employing a nanocrystal-polymer composite electrolyte modified with water and ethanol. *Nanotechnology* **2009**, *20*, No. 105204.
- (23) Bella, F.; Gerbaldi, C.; Barolo, C.; Grätzel, M. Aqueous dye-sensitized solar cells. *Chem Soc Rev.* **2015**, *44*, 3431–3473.
- (24) Arakawa, H.; Yamaguchi, T.; Sutou, T.; et al. Efficient dye-sensitized solar cell sub-modules. *Curr. Appl. Phys.* **2010**, *10*, S157–S160.
- (25) Daeneke, T.; Uemura, Y.; Duffy, N. W.; et al. Aqueous dye-sensitized solar cell electrolytes based on the ferricyanide-ferrocyanide redox couple. *Adv. Mater.* **2012**, *24*, 1222–1225.
- (26) Svensson, P. H.; Kloo, L. Synthesis, structure, and bonding in polyiodide and metal iodide-iodene systems. *Chem. Rev.* **2003**, *103*, 1649–1684.
- (27) Yang, P.; Liu, L.; Li, L.; Hou, J.; Xu, Y.; Ren, X.; An, M.; Li, N. Gel polymer electrolyte based on polyvinylidene fluoride-co-hexafluoropropylene and ionic liquid for lithium ion battery. *Electrochim. Acta* **2014**, *115*, 454–460.
- (28) Stathatos, E.; Lianos, P.; Lavrencic-Stangar, U.; Orel, B. A high-performance solid-state dye-sensitized photoelectrochemical cell employing a nanocomposite gel electrolyte made by the sol-gel route. *Adv. Mater.* **2002**, *14*, 354–357.
- (29) Bohnke, O.; Rousselot, C.; Gillet, P. A.; Truche, C. Gel electrolyte for solid-state electrochromic cell. *J. Electrochem. Soc.* **1992**, *139*, 1862–1865.
- (30) Kubo, W.; Murakoshi, K.; Kitamura, T.; Yoshida, S.; Haruki, M.; Hanabusa, K.; Shirai, H.; Wada, Y.; Yanagida, S. Quasi-solid-state dye-sensitized TiO<sub>2</sub> solar cells: Effective charge transport in mesoporous space filled with gel electrolytes containing iodide and iodine. *J. Phys. Chem. B* **2001**, *105*, 12809–12815.
- (31) Appetecchi, G. B.; Croce, F.; Scrosati, B. Kinetics and stability of the lithium electrode in poly(methylmethacrylate)-based gel electrolytes. *Electrochim. Acta* **1995**, *40*, 991–997.
- (32) Soni, S. S.; Fadadu, K. B.; Gibaud, A. Ionic conductivity through thermoresponsive polymer gel: ordering matters. *Langmuir* **2012**, *28*, 751–756.
- (33) Zhang, J.; Liu, J.; Wang, Z.; Hao, S.; Song, H. Gelation, liquid crystalline behaviour, and ionic conductivity of nanocomposite ionogel electrolytes based on attapulgite nanorods. *Langmuir* **2020**, *36*, 9818–9826.
- (34) Salikolimi, K.; Sudhakar, A. A.; Ishida, Y. Functional ionic liquid crystals. *Langmuir* **2020**, *36*, 11702–11731.
- (35) Ji, J. M.; Zhou, H.; Eom, Y. K.; Kim, C. H.; Kim, H. K. 14.2% efficiency dye-sensitized solar cells by co-sensitizing novel thieno[3,2-b]indole-based organic dyes with a promising porphyrin sensitizer. *Adv. Energy Mater.* **2020**, *10*, No. 2000124.
- (36) Nishshanke, G. B. M. M.; Arof, A. K.; Bandara, T. M. W. J. Review on mixed cation effect in gel polymer electrolytes for quasi solid-state dye-sensitized solar cells. *Ionics* **2020**, *26*, 3685–3704.
- (37) Jhong, H.-R.; Wong, D. S.-H.; Wan, C.-C.; Wang, Y.-Y.; Wei, T.-C. A novel deep eutectic solvent-based ionic liquid used as electrolyte for dye sensitized solar cells. *Electrochim. Commun.* **2009**, *11*, 209–211.
- (38) Buraidah, M. H.; Shah, S.; Teo, L. P.; Chowdhury, F. I.; Careem, M. A.; Albinsson, I.; Mellander, B.-E.; Arof, A. K. High efficient dye sensitized solar cells using phthaloylchitosan based gel polymer electrolytes. *Electrochim. Acta* **2017**, *245*, 846–853.
- (39) Bandara, T. M. W. J.; DeSilva, L. A.; Ratnasekera, J. L.; et al. High efficiency dye-sensitized solar cell based on a novel gel polymer electrolyte containing RbI and tetrahexylammonium iodide (Hex<sub>4</sub>NI) salts and multi-layered photoelectrodes of TiO<sub>2</sub> nanoparticles. *Renewable Sustainable Energy Rev.* **2019**, *103*, 282–290.
- (40) Albayrak, C.; Cihaner, A.; Dag, Ö. A new, highly conductive, lithium salt/nonionic surfactant, lyotropic liquid-crystalline mesophase and its application. *Chem. - Eur. J.* **2012**, *18*, 4190–4194.
- (41) Yilmaz, E.; Olutaş, E. B.; Barım, G.; Bandara, J.; Dag, Ö. Lithium salt–nonionic surfactant lyotropic liquid crystalline gel-electrolytes with redox couple for dye sensitized solar cells. *RSC Adv.* **2016**, *6*, 97430–97437.
- (42) Balci, F. M.; Balci, S.; Kocabas, C.; Dag, Ö. Lyotropic liquid-crystalline mesophase of lithium triflate–nonionic surfactant as gel

electrolyte for graphene optical modulator. *J. Phys. Chem. C* **2017**, *121*, 11194–11200.

(43) Barim, G.; Albayrak, C.; Yilmaz, E.; Dag, Ö. Highly conducting lyotropic liquid crystalline mesophases of pluronics (P65, P85, P103, and P123) and hydrated lithium salts (LiCl and LiNO<sub>3</sub>). *Langmuir* **2014**, *30*, 6938–6945.

(44) Albayrak, C.; Barim, G.; Dag, Ö. Lyotropic liquid crystal to soft mesocrystal transformation in hydrated salt-surfactant mixtures. *Chem. - Eur. J.* **2013**, *19*, 15026–15035.

(45) Stergiopoulos, T.; Rozi, E.; Karagianni, C. S.; Falaras, P. Influence of electrolyte co-additives on the performance of dye-sensitized solar cells. *Nanoscale Res. Lett.* **2011**, *6*, No. 307.

(46) Nakade, S.; Kanzaki, T.; Kubo, W.; Kitamura, T.; Wada, Y.; Yanagida, S. Role of electrolytes on charge recombination in dye-sensitized TiO<sub>2</sub> solar cell: the case of solar cells using the I<sup>-</sup>/I<sub>3</sub><sup>-</sup> redox couple. *J. Phys. Chem. B* **2005**, *109*, 3480–3487.

(47) Ramette, R. W.; Sandford, R. W. Thermodynamics of iodine solubility and triiodide ion formation in water and deuterium oxide. *J. Am. Chem. Soc.* **1965**, *87*, 5001–5005.

(48) Bentley, C. L.; Bonf, A. M.; Hollenkamp, A. F.; Mahon, R. J.; Zhang, J. Voltammetric determination of the iodide/iodene formal potential and triiodide stability constant in conventional and ionic liquid media. *J. Phys. Chem. C* **2015**, *119*, 22392–22403.

(49) Awtrey, A. D.; Connick, R. E. The absorption spectra of I<sub>2</sub>, I<sub>3</sub><sup>-</sup>, I<sup>-</sup>, IO<sub>3</sub><sup>-</sup>, S<sub>4</sub>O<sub>6</sub><sup>=</sup>, S<sub>2</sub>O<sub>3</sub><sup>=</sup>. Heat of the reaction I<sub>3</sub><sup>-</sup> = I<sub>2</sub> + I<sup>-</sup>. *J. Am. Chem. Soc.* **1951**, *73*, 1842–1843.

(50) Isci, H.; Mason, W. R. Electronic and magnetic circular dichroism spectra of the triiodide Ion. *Inorg. Chem.* **1985**, *24*, 271–274.

(51) De Angelis, F.; Fantacci, S.; Mosconi, E.; Nazeeruddin, M. K.; Grätzel, M. Absorption spectra and excited state energy levels of the N719 dye on TiO<sub>2</sub> in dye-sensitized solar cell models. *J. Phys. Chem. C* **2011**, *115*, 8825–8831.